Volume 1 | Number 1 | Jan 2013 | Pages 1–100

Journal of
Materials Chemistry A

Materials for energy and sustainability
www.rsc.org/materialsA

Li⁺

ROYAL SOCIETY
OF CHEMISTRY

ROYAL SOCIETY
OF CHEMISTRY

www.rsc.org/materialsA

Journal Name

ARTICLE

Derivatized cardo-polyetherketone anion exchange membranes for all-vanadium redox flow batteries

Sukhwan Yun, Javier Parrondo and Vijay Ramani[*]

Cardo-polyethereketone (PEK-C) based anion exchange membranes (AEMs) were synthesized by chloromethylation of PEK-C followed by quaternization using trimethylamine (TMA). The ion exchange capacity (IEC) of the AEM was 1.4 ± 0.1 mmol g^{-1}. The sulfate ion conductivity and Vanadium (IV) permeability were 5.6 ± 0.5 mS cm^{-1} and $8.2 \pm 0.2 \times 10^{-9}$ cm^2 s^{-1} at 30°C. The chemical stability and mechanical integrity of the AEMs were investigated upon exposure to 1.5 M VO$_2^+$ solution by monitoring the ionic conductivity, ultimate tensile strength, elongation at break, and chemical structure over 1500 hours. 1-D and 2-D NMR spectroscopy confirmed the chemical stability of the AEM over this period. The ionic conductivity of the AEM decreased from 5.6 to 4.4 mS cm^{-1} over the first 48 hours but subsequently stabilized and was reversible, while the ultimate tensile strength and the elongation at break were reduced by ca. 35%. The PEK-C based AEMs were stable during operation in a vanadium redox flow battery (VRFB) for 100 hours of testing. The coulombic and energy efficiencies of the VRFB were 98% and 80%, respectively. Post-mortem analysis of the AEM using 1-D and 2-D NMR spectroscopy showed a 15% reduction in the number of quaternary ammonium groups in the AEM.

Introduction

There has been a recent resurgence in interest in redox flow batteries (RFBs) as a consequence of the rapid development of renewable electricity plants, such as wind and solar farms. Since both wind and solar farms are intermittent (as opposed to base-load) generators, there is a need for an appropriate storage buffer to modulate spikes and slumps in energy production and demand. RFBs are modular and can be easily scaled up. Additionally, power and energy are decoupled in an RFB, which lends this technology to applications requiring large-scale electric energy storage. Examples include solar energy storage systems[1-4] and MW-scale smart grids.[3-5] In a RFB, the energy is stored in reversible redox couples that are recirculated through the electrodes of the battery during the charging/discharging process.[6] The storage of the redox species is done in external tanks allowing the independent manipulation of capacity, energy and power densities.

There are many different types of RFB systems extant and they can be classified based on the redox couples they employ: all vanadium,[1, 6-11] iron-vanadium,[12-14] iron-chromium,[6, 15-18] polysulfide-bromine,[6, 19, 20] zinc-nickel,[21] zinc-bromine[22] and zinc-cerium.[22-24] To date, all-vanadium RFB (VRFB), polysulfide-bromine RFB, and zinc-bromine RFB have made it to higher levels of technological readiness.[3, 21] Among those batteries, the all vanadium RFB uses the same element (V) in both electrode compartments. Hence, the intermixing of positive and negative electrode solutions does not cause irreversible damage to the battery. The electrolytes can be regenerated electrochemically by simply charging the battery again, facilitating the reuse of the redox solutions.[7, 25]

The ion exchange membrane (IEM) used as the separator between the compartments of RFBs plays a significant role in dictating RFB efficiencies and performance. The IEM should have high ionic conductivity, low permeability of the redox species, and good chemical and mechanical stability under RFB operating conditions. Perfluorosulfonicacid-based cation exchange membranes (e.g. Fumapem®, Nafion® and 3M membranes) have been traditionally used as separators in RFBs because of their high proton conductivity and excellent chemical stability. However, such membranes have some disadvantages, such as elevated cost and relatively high permeation of vanadium ions, resulting in self discharge of the battery.[7, 26] On the other hand, IEMs based on aromatic hydrocarbon polymers have advantages such as lower cost and perhaps lower permeation levels, and they provide reasonable thermal, chemical and mechanical stability.[27]

IEMs can be categorized as cation exchange membranes (CEMs) or anion exchange membranes (AEMs), depending on the fixed groups attached to the polymer backbone. CEMs contain fixed groups that are negatively charged (typically sulfonic acid), and transport positively charged ions such as protons and sodium ions. AEMs have positively charged fixed groups and transport negatively charged ions such as chloride, sulfate and hydroxide ions. The use of CEMs in RFBs results in cation intermixing across the chambers of the battery since the CEM cannot discriminate between the different cation species, leading to poor permselectivity.[11, 28] AEMs on the other hand exclude cations (Donnan exclusion)[29] and selectively transport anions to balance charge. Despite the promising characteristics of the AEM, there are relatively few studies related to the use of AEMs for the VRFB.[7, 9, 25, 30-36]

Several polymer such as polysulfone,[37, 38] poly(fluorenyl ether),[9] poly(arylene ether),[39, 40] poly(phthalazinone ether sulfone ketone),[41] poly(ether sulfone)-Cardo[42] and poly(ether ether ketone)[43, 44] have been used for the synthesis of AEMs.[45] The ionic conductivity, and chemical, thermal and mechanical stabilities of AEM are the critical properties that need to be improved and are usually emphasized in the study of AEMs applied to fuel cells, electrolyzers, and VRFBs.[46] For example, Tanaka et al. synthesized poly(arylene ether) based multiblock copolymers which showed significantly higher than normal hydroxide ion conductivity, up to 144 mS cm^{-1} at 80ºC, while maintaining good mechanical strength.[39] Fang et al. prepared AEMs based on poly(phthalazinone ether sulfone ketone) and these membranes also exhibited similar hydroxide ion conductivities (140 mS cm^{-1}, at 80ºC with 2 M KOH solution) with good thermal stability below 150°C.[41] Jung et al. studied the mechanical and chemical stability of polysulfone based AEMs under VRFB operating conditions, and the prepared membranes remained chemically stable in vanadium (V) solution for 3 months.[35]

For VRFB applications, it is desired that the membrane separators exhibit the low vanadium ion permeability, good chemical stability upon exposure to the various vanadium redox states, and reasonable ionic conductivities. Early studies of VRFBs employing commercially available AEMs were reported by Mohammadi and Skyllas-Kazacos.[47] The Selemion® AMV (Asahi Glass, Japan) membrane showed low chemical stability in the VRFB, while New Selemion® (type 2) showed negligible weight loss and almost constant conductivity and vanadium permeability when exposed to VO_2^+ for six months.[32] Hwang et al. studied crosslinked New Selemion® (type 2) membranes prepared using electron radiation and achieved an overall energy efficiency (EE) of 82%.[30] Jian and his group investigated chloromethylated/quaternized poly(phthalazinone ether ketone),[48] poly(phthalazinone ether sulfone),[33] and poly(phthalazinone ether ketone ketone)[34] AEMs containing trimethylammonium cations (TMA$^+$) for VRFB applications. Those AEMs allowed coulombic efficiencies (CE) between 95% and 99% during VRFB operation and exhibited vanadium (IV) membrane permeabilites between 1×10^{-7} and 4×10^{-7} cm^2 s^{-1}. Qu et al.

prepared polysulfone based AEM by quaternization using triethylamine and achieved an order of magnitude reduction in VO_2^+ permeability (1.6×10^{-8} cm^2 s^{-1}) in these membranes compared to Nafion® membranes.[31] Their VRFB exhibited stable operation over 80 cycles with CE and EE of 99% and 81%, respectively. In more recent work, Hickner et al. prepared quaternary ammonium functionalized poly(fluorenyl ether) AEMs with the extremely low VO_2^+ permeability (no detectable vanadium ion after one month), which provided 100% CE.[9] Zhao and his research group prepared silica nanocomposite AEM via an in situ sol-gel reaction and they achieved a CE and EE of 92% and 73% at a current density of 40 mA cm^{-2}.[49] In general, many of these studies focused either on performance (conductivity, permeability, CE, EE etc.) or on chemical or mechanical stability. However, it is necessary to examine both aspects, including the effect of in situ operation on AEM stability, to demonstrate the feasibility of AEMs for practical VRFB operation.[35] This study adopts an in-depth approach encompassing both performance and stability aspects of AEM use in a VRFB.

Among the family of poly(aryl ether ketone)s cardo-polyetherketone (PEK-C) is a material with suitable properties for the synthesis of electrolyte membranes for electrochemical systems.[50] PEK-C based CEMs have been prepared by sulfonation.[51-55] Recently, the synthesis of AEMs by chloromethylation of PEK-C followed by displacement of the chloride by reaction with tertiary amine (quaternarization) has been reported.[10, 56] These studies proposed the possibility of using PEK-C based IEMs in applications including pervaporation, nanofiltration, and alkaline and hydrogen fuel cell systems. In this work, we evaluate, for the first time, the use of quaternary ammonium functionalized PEK-C for VRFB applications.

The initial assessment of the suitability of PEK-C based AEMs for VRFB applications was performed by studying the changes in AEM ion exchange capacity (IEC), ionic conductivity, vanadium (IV) permeability, ultimate tensile stress, and changes in AEM composition, measured using nuclear magnetic resonance (NMR), after immersion during 60 days in 1.5 M VO_2^+ solution in 3M H_2SO_4. For the stability test, we selected a solution with the same composition as employed in a VRFB, and chose VO_2^+ because it is the most oxidizing species present in the electrolyte solutions. The AEM was also evaluated in an operating VRFB by charging/discharging for 100 hours (about 20 cycles). Post-mortem analysis of the VRFB-tested membrane was conducted to investigate the occurrence (and extent) of any chemical and/or mechanical degradation as a consequence of VRFB operation. Multiple spectroscopy tools such as Fourier transform infrared spectroscopy (FTIR), ^{1}H NMR, ^{13}C NMR, two-dimensional NMR correlation spectroscopy (COSY), and ^{1}H-^{13}C heteronuclear multiple quantum correlation (HMQC) spectroscopy were employed to characterize the polymers during the synthesis steps, to investigate changes in the polymer composition upon exposure to VO_2^+ solutions, and to identify any possible degradation products as an initial step in postulating degradation mechanisms. The information provided in this study will provide fundamental insights relevant to the development of advanced AEMs for VRFB applications.

Experimental methods

Synthesis of chloromethylated PEK-C and PEK-C based AEMs

10 g of PEK-C (Xuzhou Vat Chemical Company, China) was dissolved in 500 mL of chloroform (>99.8%, Fisher Scientific). After complete dissolution of the polymer, 6 g of paraformaldehyde (96%, Acros), 25 mL of chlorotrimethylsilane (98%, Acros) and 0.47 mL of tin tetrachloride (>99%, Sigma Aldrich) were added under mild stirring. The reaction mixture was kept at 80°C for a week. The reaction time and concentration of reactants were optimized to obtain a chloromethylated polymer with a degree of chloromethylation (DF, chloromethyl groups per polymer repeating unit) of 0.8-0.9. The reaction was stopped by precipitation of the polymer in methanol (4 times the volume of the reaction mixture). The precipitate was recovered by centrifugation (Thermo Scentific, Multifuge X1) at 5000 rpm for 10 min, and purified by redissolving in dimethylformamide (Acros Organics) followed by precipitation in methanol.

The quaternary ammonium cardo-PEK anion exchange membrane in the chloride counter-ion form (QPEK-C-TMA$^+$ Cl$^-$) was obtained by reaction of chloromethylated PEK-C (CMPEK-C) with trimethylamine (TMA).[27, 45, 56-60] The reaction was carried out at 30°C using dimethylformamide as the solvent. Thin film membranes were obtained by casting the reaction solution onto a glass plate (3" x 3") in an oven at 70°C on a leveled surface. The plates were kept in the oven overnight to allow complete evaporation of the solvent. Membranes of approximately 40 μm thickness were prepared.

QPEK-C-TMA$^+$ Cl$^-$ films were ion exchanged to the SO$_4^{2-}$ counter-ion form by immersing in 1 M Na$_2$SO$_4$ solution at room temperature for 24 hours. The solution was changed several times to improve the ion exchange process. After ion exchange, the resultant QPEK-C-TMA$^+$ SO$_4^{2-}$ membranes were rinsed with an abundant amount of DI water for 4 hours to remove residual salts.

Gel permeation chromatography

The molecular weights (number-average molecular weight; Mn, and weight-average molecular weight; Mw) of the polymers were determined by gel permeation chromatography (GPC). The measurements were performed in a Waters chromatographic instrument equipped with a 510 HPLC pump, a 410 differential refractometer, and a 486 Tunable absorbance detector. Polystyrene standards were used to calibrate the molecular weights. The polymer samples were dissolved in tetrahydrofuran prior to measurement (concentration 1 g/L) and injected into the instrument.

NMR spectroscopy

NMR measurements were performed on a Bruker Avance 360 MHz NMR spectrometer. The NMR experiments performed were as follows: 1-D ^{1}H (spectra collected at 360 MHz), ^{13}C (spectra collected at 90 MHz – proton decoupled), and 2-D ^{1}H-^{1}H COSY, and ^{1}H-^{13}C HMQC. 1-D and 2-D NMR techniques have been applied to investigate the degradation of AEMs immersed in oxidizing solutions.[35, 38, 61, 62] The sample was prepared by dissolving approximately 50 mg of the polymer in 0.85 mL of deuterated solvent. We used dimethylsulfoxide (DMSO-d$_6$) to dissolve the AEMs and chloroform (CHCl$_3$-d$_6$) to dissolve PEK-C and chloromethylated polymers. The selection of the solvents was based on the material solubility. 35 mL of tetramethylsilane (TMS) was added as internal standard to all samples.

IEC

The IEC of the AEMs was measured by titration and also estimated from ^{1}H NMR spectra. For the titration method, 0.1-0.15 g of QPEK-C-TMA$^+$ Cl$^-$ was used. The sample was exchanged to the chloride counter-ion form by immersion in 1 M NaCl solution overnight. The membrane was rinsed with abundant DI water several times to remove the residual chloride on the surface. The membrane was then immersed in 1 M Na$_2$NO$_3$ solution to exchange the chloride ions. The solution containing the chloride ions was titrated against 0.05 M AgNO$_3$ solution. The end-point was determined potentiometrically using an Ag/AgCl working electrode and an Ag/AgCl reference electrode immersed in the solution. IEC was determined by using the following equation:

$$IEC_{titr} = (0.05 \times V_{eq})/m \qquad [1]$$

where V_{eq} is the volume of 0.05 M AgNO$_3$ added to reach the equivalence point (mL), m is the dry weight of the membrane (g), and IEC_{titr} is the IEC estimated by titration method.

For the method using 1H NMR spectra, the IEC was estimated from ^{1}H NMR spectra by comparing the area corresponding to the protons in -CH$_2$Cl moiety and the aromatic protons in the polymer backbone (DF value). The DF was estimated by the following equation:

$$DF = \frac{N_{H,a}}{N_{H,c}} \times \frac{A_c}{A_a} \qquad [2]$$

where $N_{H,a}$ and $N_{H,c}$ are the number of hydrogen attached to the aromatic rings and chloromethyl groups, respectively, ($N_{H,a}$=19 and $N_{H,c}$=2 for QPEK-C-TMA$^+$), A_a and A_c are the areas in ^{1}H NMR spectra corresponding to the aromatic protons in the polymer backbone and to the protons in –CH$_2$Cl moiety, respectively.

The following equation was used to estimate the IEC from the ^{1}H NMR spectrum:

$$IEC = \frac{DF \times 1000}{[MW_{PEK-C} + DF\,(MW_{base} + MW_{cation} + 14 - 1)]} \qquad [3]$$

where DF is degree of functionalization, MW_{PEK-C}, MW_{base}, and MW_{cation} are the molecular weights of PEK-C repeat unit, TMA, and counter cation (Cl$^-$ or SO$_4^{2-}$) respectively.

Ionic conductivity

The in-plane ionic conductivity of the membranes was measured using electrochemical impedance spectroscopy. A membrane sample (with an approximate size of 1 cm x 3 cm) was placed in a 4-point conductivity cell with platinum electrodes (BekkTech, LLC) and immersed in deionized water in a thermostatic bath. A Gamry potentiostat (Series G750) was used to measure the in-plane impedance of the membrane in the frequency range 100,000 Hz to 0.1 Hz. The high frequency resistance, together with the distance between the electrodes, and the thickness and width of the membrane (collectively, the cell constant) was used to calculate the membrane ionic conductivity:

$$\sigma = L / (R \times t \times w) \qquad [4]$$

where σ is the in-plane conductivity, R is the high frequency resistance, and t and w are thickness and width of membrane (measured in the fully hydrated membrane).

Water uptake

Water uptake was measured both in liquid phase and in vapor phase. For the water uptake measurement in the liquid phase, samples in the sulfate counter ion form were dried in a vacuum oven overnight and weighed. The samples were immersed in deionized water and stored in an oven set to either 30°C or 60°C. After 24 hours, the samples were quickly swabbed to remove liquid from the surface. The sample weight was then measured. The following equation was used to estimate the water uptake (liquid-phase):

$$WU(wt\%) = \frac{W_{hydrated} - W_{dry}}{W_{dry}} \times 100\% \qquad [5]$$

where WU is the water uptake, $W_{hydrated}$ and W_{dry} are the measured weight of the samples in hydrated and dry condition, respectively.

Vanadium (IV) permeability

To measure the vanadium permeability, the membrane was placed between two compartments of a diffusion cell (20 mL diffusion cell from PermeGear Inc. with an effective area of 4.91cm²). The top compartment was filled with 10 mL of 1.5 M $VOSO_4$ in 3 M H_2SO_4 and the bottom compartment was filled with 20 mL of 1.5 M Na_2SO_4 in 3 M H_2SO_4 solution. Samples from the diluted side (Na_2SO_4 solution) were withdrawn at predetermined time intervals. The absorbance of this solution was measured at a wavelength of 745 nm and used to estimate the concentration of VO^{2+} using a previously obtained calibration curve. Vanadium ion permeability was determined using the following equation:

$$P = \frac{V_B \times d}{C_A \times A} \times \frac{dC_B}{dt} \qquad [6]$$

where P is the permeability, V_B is the volume of solution in the diluted side (20 mL), d is the thickness of the membrane, C_A is the concentration of VO_2SO_4 in the concentrated side (1.5M), A is the effective area of membrane exposed to the solution (4.91 cm²) and dC_B/dt is the change of the concentration with time (measured from the experimental data).

Thermogravimetric analysis (TGA) and differential scanning calorimetry (DSC)

TGA was used to study the thermal stability of and onset of decomposition in PEK-C, CMPEK-C, and QPEK-C-TMA⁺ SO_4^{2-} membranes. The experiment was performed in a Discovery TGA series thermogravimetric analyzer (TA instruments) using a high resolution scan program at 50°C min⁻¹ (this program is approximately equivalent to a constant scan rate program at 10°C min⁻¹ but it adjusts the scan rate depending on the rate of weight loss and hence it is faster). The experiments were performed while purging the furnace with nitrogen gas (50 mL min⁻¹).

A modulated DSC (Q series DSC; TA instruments) was used to identify phase transitions and assist in the characterization of the various membranes. Approximately 2 mg of the polymer (PEK-C or QPEK-C-TMA⁺ SO_4^{2-}) was placed in a T-zero (TA instruments) pan previously. Samples were first heated to 190°C at 10°C min⁻¹, maintained at 190°C for 5 minutes, and quenched to 0°C. The samples were then heated to 300°C and 250°C for PEK-C and QPEK-C-TMA⁺, respectively. The scan rate for heating was 2°C min⁻¹, and the temperature modulation amplitude was 1°C with a period of 60 s. Nitrogen was used as the purge gas (50 mL min⁻¹). The maximum temperature was selected to be approximately 20°C below the onset temperature for degradation of the polymer as ascertained from the TGA scans.

Dynamic mechanical analysis (DMA)

DMA was used to determine the storage and loss modulus of the polymers and to estimate the glass transition temperature. A Q800 differential mechanical analyzer (TA instruments) equipped with a liquid nitrogen cooling accessory was used to perform the experiments. The temperature was ramped from 25 to 300°C at a rate of 3°C min⁻¹ and the storage and loss modulus were measured at a frequency of 1 Hz. The membrane (approximate dimensions: 50 mm × 5 mm × 0.05 mm) was fixed in a film tension clamp using a torque of 3 lbF × in, and exposed to a sinusoidal deformation with an amplitude of 0.1% of its length. A preload force of 0.1N was used (to keep the membrane under tension at all times). The glass transition temperature was identified by a sharp decrease of storage modulus and a maximum (peak) observed in loss modulus and tangent of delta (tan δ). The glass transition temperatures obtained were compared with corresponding values obtained from modulated DSC data.

Tensile tests were performed to investigate changes in the mechanical properties of the polymer after exposure to vanadium solutions. The membrane (approximate dimensions: 50 mm × 5 mm × 0.05 mm) was fixed in a film tension clamp using a torque of 3 lbF × in, and heated to 50°C under 50 % RH. The membrane was allowed to equilibrate for 60 minutes

before starting the test. The tensile test was performed by stretching the membrane at 0.5 MPa min^{-1} until failure. The stress-strain curves are reported, along with the Young's modulus, which was estimated from the slope of the linear portion of the stress-strain curve.

AEM oxidative stability test

The *ex-situ* oxidative stability of the AEM was investigated by immersing QPEK-C-TMA$^+$ SO$_4{}^{2-}$ membrane samples in 1.5 M (VO$_2$)$_2$SO$_4$ in 3 M H$_2$SO$_4$. The stability test was performed at a temperature of 30°C, which was higher than room temperature, to account for the internal heating of the cell due to irreversible losses during room temperature operation. The degradation process of the membrane was monitored periodically by measuring the ionic conductivity and NMR after exposure times of 2, 7, 14, 30 and 60 days. The stability of the membranes was evaluated by monitoring ionic conductivity, ultimate tensile stress, elongation at break, Young's modulus and chemical structure via NMR (^{1}H NMR, COSY and ^{1}H-^{13}C HMQC).

Single cell VRFB tests

Single cell RFB testing was carried out in a 10 cm^2 acid-resistant hardware (Fuel Cell Technologies, Inc). The single cell was assembled by sandwiching a membrane between two carbon felt electrodes (Alfa Aesar) that were activated by heating in air at 400°C for 30 h.[63] VRFB testing was performed using 1.5 M V^{2+}/V^{3+} and 1.5 M VO^{2+}/VO$_2{}^+$ as the negative and positive electrolytes, respectively, both in 3 M H$_2$SO$_4$ solution. The solutions were recirculated using two peristaltic pumps. The active area of the cell was 10cm^2 and the volume of electrolyte solution used was 20mL in each half-cell. Charge-discharge tests were conducted at a constant current density of 30mA cm^{-2} at 25°C. The cutoff voltages for the charge (upper limit) and discharge (lower limit) cycles were 1.65 and 0.65V, respectively. The maximum cut-off voltage used during charging (1.65 V) was selected based on the maximum potential the battery could hold without excessive hydrogen evolution. The lower cut-off cell voltage during discharge (0.65V) was selected on the basis of allowing complete discharge of the flow battery. The CE was defined as the discharge capacity (A h) divided by the charge capacity (A h). The EE was defined as the discharge energy (W h) divided by the charge energy (W h), and the voltage efficiency (VE) was calculated as VE = EE/CE.[31]

Results and discussion

Characterization of CMPEK-C and QPEK-C-TMA$^+$

PEK-C (From GPC: Mn≈38,500 and Mw≈90,700) based AEMs were synthesized by chloromethylation of PEK-C followed by quaternization using TMA (Figure 1). PEK-C based AEMs were first prepared by Xiong *et al.*[56] However, they assigned the ^{1}H NMR peak at 2.2ppm to the protons in the

chloromethyl moiety. Based on our own results, and several other results in the literature,[27, 33-35, 59, 64] we believe this assignment to be incorrect. In fact, the protons in the chloromethyl moiety adjacent to aromatic ring in a polyether aromatic polymer should be placed between 4.4 and 4.9 ppm. In this study, a peak at 4.5-4.6 ppm was observed after chloromethylation of PEK-C. This peak remained at the same position after quaternerization of the chloromethylated polymer with TMA, and a new peak, corresponding to –CH$_3$ groups attached to quaternary ammonium, appeared at approximately 3.15 ppm (Figure S1c). The ratio of the areas of the peak at 4.5 ppm (assigned to -CH$_2$-) and at 3.15ppm [assigned to N-(CH$_3$)$_3$] was approximately 4.5, which matched well with the relative number of protons at positions "4" and "5" in the AEM. This evidence was sufficient to confirm the occurance of chloromethylation of PEK-C and subsequent reaction with TMA to form the quaternerized AEM. The presence of TMA groups from the quaternary ammonium cation was also confirmed through FTIR (see Figure S2). The ^{1}H NMR peak labels used are shown in Figure S1. The NMR chemical shifts for the methylene bridge moieties in CMPEK-C and QPEK-C-TMA$^+$ was placed between 4.4 and 4.8 ppm. The CMPEK-C had a DF of 0.9, as calculated from the NMR spectra. The error associated with this calculation typically varies from 5-20%.[65]
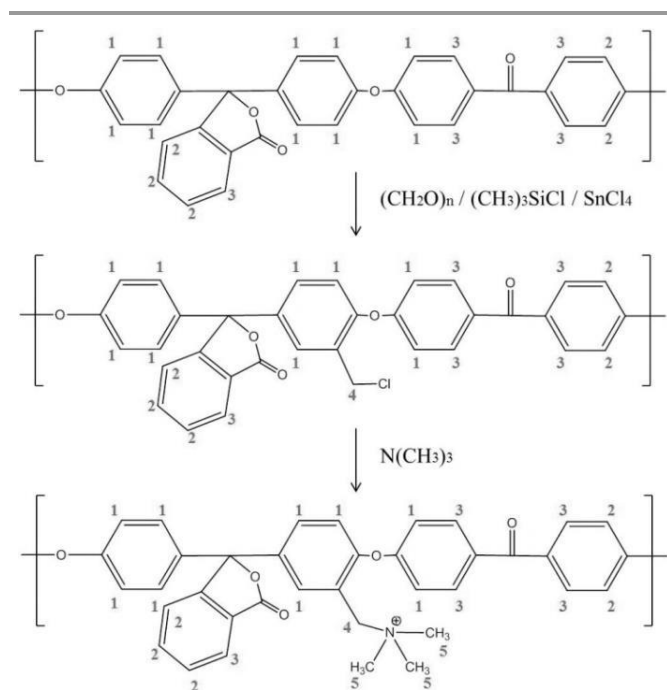

Figure 1. Synthesis of quaternenized AEMs from PEK-C

IEC, ion conductivity, water uptake, and vanadium (IV) permeability

The IEC of QPEK-C-TMA$^+$ as measured by titration was 1.54 mmol g^{-1} for the chloride counter-ion form (and 1.41 mmol g^{-1} for the sulfate form). The IEC was also estimated from the DF value of the CMPEK-C. Equation 3 was used in this calculation, and yielded IEC values of 1.51 mmol g^{-1} and 1.38 mmol g^{-1} for

the chloride and sulfate counter-ion forms, respectively. The values obtained by these two methods were in close agreement.

AEMs exhibit lower ionic conductivity than PEMs due to the lower mobility of anions compared to protons.[9] The ionic conductivity of QMPEK-C-TMA$^+$ membranes (with SO$_4^{2-}$ as counter ion, measured in deionized water) ranged between 5 to 20 mS cm^{-1}, increasing with temperature (Table 1). Arrhenius behavior was observed, with activation energy of 21.7±0.9 kJ mol^{-1}. The ionic conductivity can be increased by increasing the DF of CMPEK-C; however, DF cannot be increased indiscriminately due to adverse consequences on AEM mechanical properties. The desired DF for CMPEK-C is between 0.9 and 1.2, which yields an equitable set of properties such ionic conductivity, vanadium permeability and chemical and mechanical stability.[25, 34, 45] Despite of the relatively low ionic conductivity (as measured in deionized water) of the QMPEK-C-TMA$^+$ membrane compared to CEMs, the high concentration of free SO$_4^{2-}$ in the electrolyte solution of VRFB should enhance this value during operation.[9]

Table1. Sulfate ion conductivity of QPEK-C-TMA$^+$ AEMs as measured in deionized water.

Temperature (°C)	SO$_4^{2-}$ conductivity (mS cm^{-1})
30	5.6±0.5
60	11.7±0.4
80	19.1±0.8

Low-moderate water uptake is a requisite to achieve a balance between ion transport and adequate AEM mechanical integrity during long term VRFB operation. Figure 2 shows the liquid-phase water uptake at 30°C and 60°C for PEK-C, CMPEK-C and QPEK-C-TMA$^+$ SO$_4^{2-}$. In line with expectations, PEK-C and CMPEK-C had extremely low water uptake due to the absence of any hydrophilic domains (both hydrocarbon and chloromethylated domains are hydrophobic). At 30°C and 60°C, the QPEK-C-TMA$^+$ SO$_4^{2-}$ had a liquid–phase water uptake of 36±2 wt% and 39±2 wt%, respectively, which are higher than Nafion® 212 (15±1 wt%) but relatively low for an AEM.[37, 64, 66, 67] Vapor-phase water uptake was also measured (Figure S3). QPEK-C-TMA$^+$ SO$_4^{2-}$ had a vapor-phase water uptake of 30wt% at 95% RH and 25°C. In general, the liquid-phase and vapor-phase water uptake data yielded similar trends. The moderate water absorption of QPEK-C-TMA$^+$ SO$_4^{2-}$ resulted from the presence of hydrophilic quaternary ammonium groups attached to the backbone. The modest DF used precluded excessive swelling.

The VO^{2+} permeability through QPEK-C-TMA$^+$ was measured to be 8.2 ±0.2 ×10^{-9} cm^2 s^{-1}. This value was 35 times lower than the corresponding permeability through Nafion® membranes (2.9 ±0.2 ×10^{-7} cm^2 s^{-1}).[32, 34, 68, 69] The reduced permeability could be explained by two phenomena: 1) the Donnan exclusion principle – in other words, the quaternary ammonium groups of QPEK-C-TMA$^+$ AEM effectively repel the positively charged vanadium ions; and 2) the presence of narrower and less connected hydrophilic channels in aromatic based ion conducting membranes when compared to perfluorinated

membranes such as Nafion®.[70] The stronger confinement of the water molecules in the narrow channels in PEK-C based polymers in combination with the Donnan exclusion lead to reduced VO^{2+} permeability. The positive effect of low vanadium permeability on VRFB performance will be discussed later.
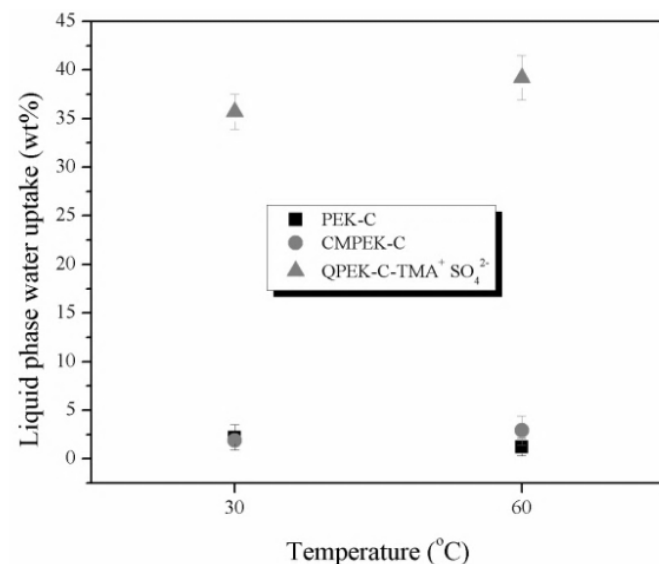

Figure 2. Liquid-phase water uptake of PEK-C, CMPEK-C and QPEK-C-TMA$^+$ SO$_4^{2-}$

Thermal and mechanical properties of PEK-C, CMPEK-C and QPEK-C-TMA$^+$ SO$_4^{2-}$ membranes

The weight-loss vs. temperature curves obtained from TGA for PEK-C, CMPEK-C and QPEK-C-TMA$^+$ SO$_4^{2-}$ are shown in Figure S4. As expected, the PEK-C exhibited the best thermal stability. The onset of degradation onset PEK-C was observed at 460°C. QPEK-C-TMA$^+$ SO$_4^{2-}$ was relatively stable, with the onset for degradation observed at 260°C. CMPEK-C had the least stability, with degradation onset observed at approximately 150°C. The increase in thermal stability upon quaternarization has been reported earlier by Liu *et al*.[64] Compared to quaternary ammonium groups, chloromethyl groups tend to be easily decomposed. The derivative curves of the thermogravimetric profile (DrTGA) (Figure S4-S6) provide more details about the thermal decomposition. The weight loss of CMPEK-C occurring between 150 and 260°C was attributed to the decomposition of -CH$_2$Cl groups. The primary weight loss of QPEK-C-TMA$^+$ SO$_4^{2-}$ was observed at temperatures around 260°C (Figure S4) which was attributed to the degradation of quaternary ammonium groups.[10, 41, 66] The rapid weight loss observed for all the membranes at around 460°C and 550°C were attributed to the decomposition of the carbon chain and phenyl group including phenolphthalein (cardo) group, which form part of the PEK-C backbone.[25, 45, 51]

DMA was used to determine the glass-transition temperatures (T$_g$) of PEK-C, CMPEK-C and QPEK-C-TMA$^+$ SO$_4^{2-}$. The sharp decrease of storage modulus and maximums seen in loss modulus and tan δ are indicators of the T$_g$ (see Figure 3). The T$_g$s obtained for PEK-C and QPEK-C-TMA$^+$ SO$_4^{2-}$ were 226°C

and 221°C, respectively. It has been reported that the T_g of the commercial PEK-C is between 218 and 228°C.[50, 52]. The T_g obtained for CMPEK-C was slightly lower (204°C). The considerable increase in storage modulus observed between 120 and 150°C for all samples indicated that the membranes underwent a transition during heating as a result of structural relocation in the glassy state.[27, 71] The exact mechanism of the structural relocation was not determined; however, the existence of the transition around 135°C was verified. The transition was also observed from DSC experiments, as discussed below.
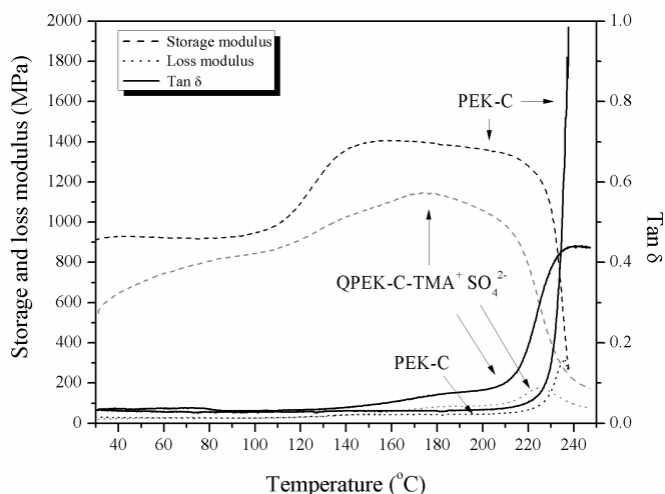

Figure 3. Dynamic mechanical analysis (DMA) of PEK-C and QPEK-C-TMA$^+$ SO$_4^{2-}$ membranes

The slope of the DSC trace for QPEK-C-TMA$^+$ SO$_4^{2-}$ was observed to change at around 68°C (Figure 4). This change was also seen for PEK-C, but was very subtle. This variation in heat flow was attributed to a secondary transition (β-transition) due to side group motion in the glassy polymer, as postulated by Liu *et al.*, who also confirmed the existence of the same transition.[71] Additionally, there was another variation observed in the DSC traces occurring between ca.140°C and 200°C. This transition was also observed in the storage modulus as measured by DMA. It was postulated that both PEK-C and QPEK-C-TMA$^+$ SO$_4^{2-}$ undergo other secondary transitions beginning at 145°C and 140°C, respectively.

The ultimate tensile strength and the elongation at break of the membranes were estimated from tensile test results. These mechanical properties changed significantly upon quaternarization. As shown in Table 2, QPEK-C-TMA$^+$ SO$_4^{2-}$ had lower ultimate tensile strength but higher elongation at break compared to PEK-C and CMPEK-C.[27] The Young's modulus of QPEK-C-TMA$^+$ SO$_4^{2-}$ membrane was around 0.5 GPa, very similar to that of Nafion® 212. The Young's modulus of AEMs has been reported to range between 0.5 GPa to 2.7 GPa.[37, 62, 64] Upon introduction of quaternary ammonium groups, to PEK-C, ion-containing domains developed within the polymer, leading to lower crystallinity and hence the lower modulus of QPEK-C-TMA$^+$ SO$_4^{2-}$.[39] The ultimate tensile

strength of QPEK-C-TMA$^+$ SO$_4^{2-}$ was comparable to Nafion® 211, confirming that it had adequate mechanical strength to be used in a VRFB.[9, 72] However the elongation at break of QPEK-C-TMA$^+$ SO$_4^{2-}$ (<20%) is much lower than Nafion® (around 180%) and this could result in membrane cracking due to fatigue during redox flow battery operation if the stack is not properly designed.
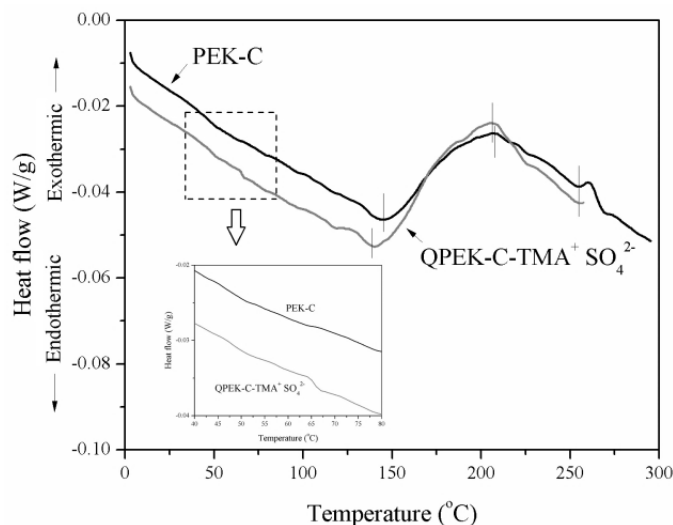

Figure 4. Modulated DSC for PEK-C and QPEK-C-TMA$^+$ SO$_4^{2-}$ AEMs

Table 2. Mechanical properties of PEK-C, CMPEK-C, and QPEK-C-TMA$^+$ SO$_4^{2-}$ measured by stress-strain test

	Ultimate tensile strength (MPa)	Elongation at break (%)	Young's modulus (GPa)
PEK-C	35 ± 2	7.9 ± 0.6	1.08 ± 0.09
CMPEK-C	33 ± 2	7.7 ± 0.4	0.97 ± 0.14
QPEK-C-TMA$^+$ SO$_4^{2-}$	19 ± 2	18.1 ± 1.4	0.54 ± 0.03
Nafion® 212	14 ± 1	178 ± 11	0.54 ± 0.03

Stability of QPEK-C-TMA$^+$ SO$_4^{2-}$ in VO$_2^+$ solution

The chemical and mechanical stability of QPEK-C-TMA$^+$ in a highly oxidizing VO$_2^+$ solution was monitored over a period of 1500 hours (2 months) (See Table 3). The yellow color of the test solution remained unchanged during this period, confirming there was no vanadium reduction reaction occurring in solution.[9, 35, 40] The color of the immersed membranes changed from clear to orange during this period. This change was attributed to the penetration of vanadium ions into the membrane.[35] Since there was no such color change when PEK-C and CMPEK-C were immersed in the same solution, the penetration of vanadium ions was associated with the presence of ionic domains inside the QPEK-C-TMA$^+$ membrane. The ionic domains associated with the quaternary ammonium group are hydrophilic and hence allow the VO^{2+} ions to be solvated by the water molecules around the quaternary ammonium groups.[35]

The ionic conductivity of QPEK-C-TMA$^+$ initially decreased with increasing immersion time (up to about 150 hours) due to

the intrusion of less mobile vanadium ions into the clusters, which hindered ion transfer by blocking ionic pathways. (Note: When the sample was washed with 3 M H_2SO_4 solution, it regained its original transparent state and its original conductivity). Subsequent to the initial decline, the ionic conductivity of QPEK-C-TMA$^+$ was maintained at about 4.4 mS cm^{-1} consistently over the 1500 hour immersion period. The same sample, after 2 months of immersion in the vanadium solution, regained its original conductivity of 5.2±0.5 mS cm^{-1} after washing with 3 M H_2SO_4 to remove the imbibed vanadium ions. This confirmed that the vanadium ion ingress was not necessarily a serious issue leading to irreversible conductivity loss, and that a stable conductivity could be obtained after some initial drop caused by occlusion of ion transport pathways.

Table 3. The effect of exposure of QPEK-C-TMA$^+$ to 1.5 M VO_2^+ (in 3M H_2SO_4 at 30ºC) on ionic conductivity and ultimate tensile strength (Note: the data from *ex-situ* post-mortem test is also included)

Time of exposure to VO_2^+ (days)	Sulfate ionic conductivity (mS cm^{-1})	Ultimate tensile strength (MPa)	Elongation at break (%)	Young's modulus (GPa)
0	5.6 ± 0.2	19 ± 2	18.1 ± 1.4	0.54 ± 0.03
2	5.7 ± 0.3	20 ± 1	11.9 ± 2.7	0.46 ± 0.06
7	4.3 ± 0.5	18 ± 1	9.7 ± 2.1	0.52 ± 0.03
14	4.4 ± 0.4	19 ± 1	10.2 ± 0.6	0.55 ± 0.02
30	4.4 ± 0.6	21 ± 1	11.4 ± 1.1	0.58 ± 0.03
60	4.3 ± 0.7	12 ± 1	8.3 ± 1.4	0.49 ± 0.04
100 hours of cycling test	4.7 ± 0.6	9±2	3.5±0.6	0.39 ± 0.08

The mechanical stability of QPEK-C-TMA$^+$ was also investigated as a function of time of exposure to VO_2^+ solution. As seen in Table 3, the ultimate tensile strength was constant during the first month of exposure to this oxidizing solution. However, the ultimate tensile strength of the sample was reduced to half its initial value after 1500 hours. We inspected the NMR spectra periodically but did not unearth any structural changes that could lead to this loss in strength. NMR is only sensitive to about ±10 mol % change in chemical composition and is often not able to detect end groups in polymers. We therefore measured the molecular weights (Mn and Mw) of QPEK-C-TMA$^+$ before and after the stability test (2 months in 1.5M VO_2^+ + 3M H_2SO_4) using GPC, and we found the post-test values to be 31,100 and 73,700, respectively, which was about 20% less than the initial values reported earlier. Since the mechanical properties of polymers are determined almost exclusively by the polymer's molecular weight, we believe that the observed loss in the mechanical properties was a resultant of the reduction in polymer molecular weight due to degradation.

A detailed 2-D NMR study was performed using the HMQC (2-D NMR) method. The ^{1}H-^{13}C HMQC spectra of QPEK-C-TMA$^+$ before and after 1500 hours of exposure to oxidizing

vanadium solution are shown in Figure 5a and 5b. The peak attributed to hydrogen and carbon in position 5 (moiety resulting from chloromethylation) does not appear in the HMQC spectrum domain, because the signal obtained from these hydrogen atoms was relatively lower than the signal obtained from the hydrogen atoms attached to aromatic ring. However, stability of the cationic site was confirmed by the absence of change of the features attributed to TMA$^+$ (position 6) groups (See Figure 5b). The identical spectra for QPEK-C-TMA$^+$ SO_4^{2-} membranes before and after exposure to the VO_2^+ solution suggested that there was no perceivable degradation in cation chemical structure induced by the acidic electrolyte solution (1.5 M VO_2SO_4 in 3M H_2SO_4) at 30ºC over 1500 hours.
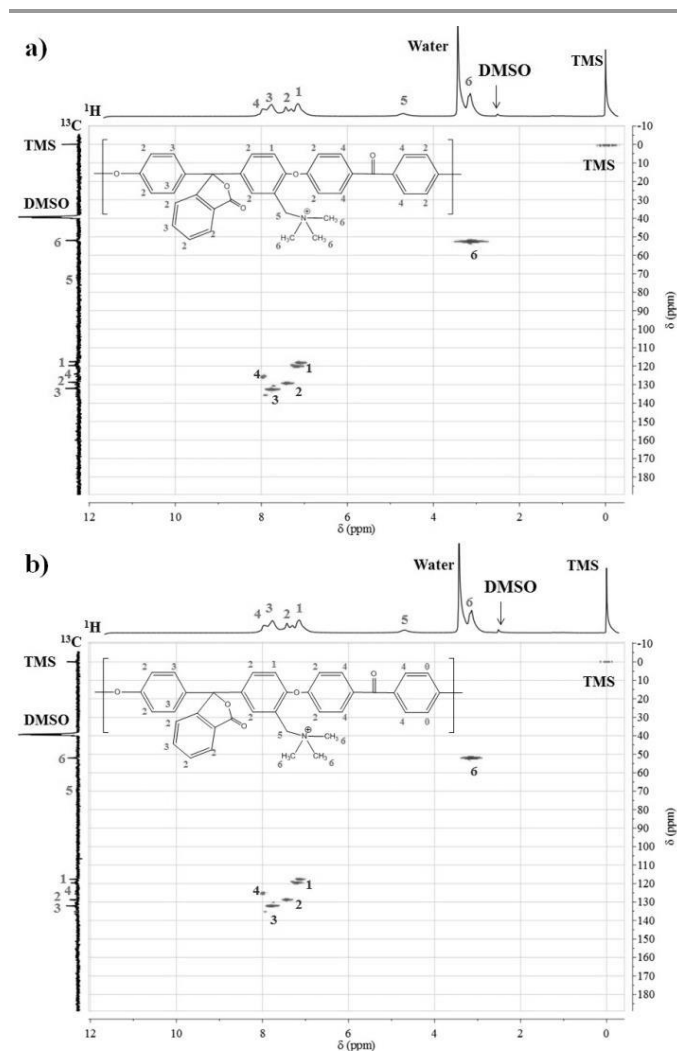

Figure 5. HMQC (1H-13C) NMR spectra of QPEK-C-TMA$^+$ a) before and b) after exposure to VO_2^+ solutions

The decrease of the polymer molecular weight was attributed to a backbone degradation mechanism. Chen *et al.* proposed the that VO_2^+ species can degrade the polymer by incorporating hydroxyl groups into the polymer's aromatic backbone, followed by the oxidation of these hydroxyl groups to quinone

functionalities through a redox mechanism.[73] The final steps involve ring opening reactions that lead to backbone degradation. The presence of ionic groups tethered to the polymer backbone can also affect backbone degradation by altering the electron density of aromatic ring.[38]

Single cell VRFB charge/discharge cycling test

Figure 6 shows the charge–discharge curves obtained on a VRFB assembled with a QPEK-C-TMA$^+$ AEM separator. The data was obtained at a current density of 30 mA cm^{-2}. At this current density, a Nafion®-212 based VRFB has been reported to exhibit lower charging voltage compared to this QPEK-C-TMA$^+$ based VRFB because of the lower resistance of the Nafion® 212 membrane to proton transport, than for the QPEK-C-TMA$^+$ membrane to sulfate ion transport.[9] However, this VRFB yielded a high discharge capacity, as a result of the extremely low vanadium ion permeability through the membrane.
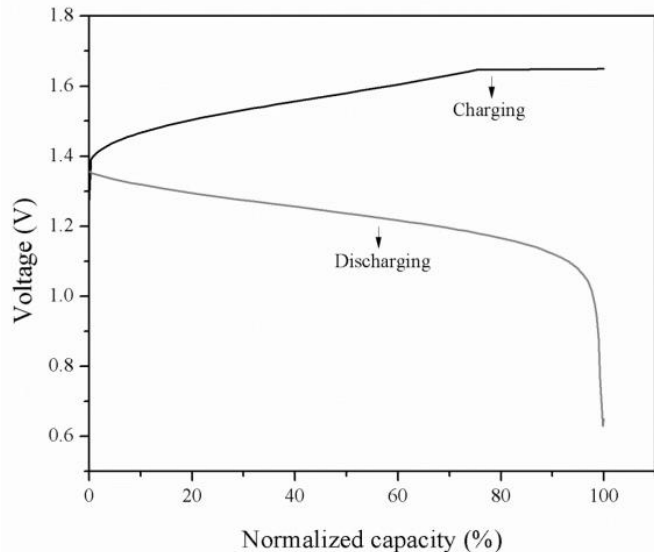

Figure6. Charge–discharge curves obtained on a VRFB prepared using a QPEK-C-TMA$^+$ AEM separator (Current density: 30 mA cm^{-2})

The VRFB prepared using the QPEK-C-TMA$^+$ AEM was operated for 100 hours (20 charge/discharge cycles). The various efficiencies are plotted in Figure 7. An acceptable EE of 78-80 % was obtained, suggesting that the QPEK-C-TMA$^+$ membranes were indeed suitable for VRFB operation. The VE is primarily determined by the membrane ohmic resistance, while the vanadium crossover flux governs the CE. Chen *et al.* prepared poly(fluorenyl ether) AEMs with extremely low vanadium permeability and 100 % CE.[9] Zhang *et al.* achieved 99% CE with their poly(phthalazinone ether ketone ketone) AEM.[34] In spite of these excellent CEs, 60% and 80% EE at 80 mA cm^{-2}, respectively, were obtained in these studies. These results are consistent with what we have observed. It is still challenge to have a higher EE in an AEM-based VRFB than in a VRFB using a CEM separator (85-90% EE reported with

Nafion® at a current density of 80mA/cm^2).[34, 40] The enhancement of sulfate ion (and similar anion) conductivity through the AEM maintaining exceptionally low vanadium ion permeability will remain an important research topic for the future.
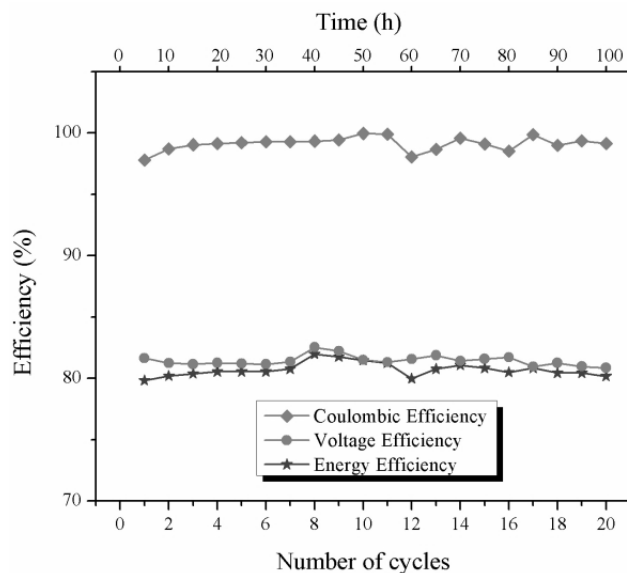

Figure 7. Coulombic, voltage and energy efficiencies obtained during charge-discharge cycling (30 mA cm-2) of a VRFB using a QPEK-C-TMA+ AEM separator (1.5 M vanadium solution in 3 M H2SO4 solution)

Post-mortem test after charge-discharge cycling test

After 20 charge/discharge cycles during about 100 hours, the cell was disassembled and post-mortem tests were performed on the AEM by measuring ionic conductivity, ultimate tensile strength and elongation at break, and the NMR spectra. Microscopy was also performed on the AEM. As shown in Figure S7, the white regions ascribed to the ionic domains became coarser after 100 hours of testing. The modification in surface topography was attributed to surface oxidation of the AEM. The ionic conductivity of the QPEK-C-TMA$^+$ SO$_4^{2-}$ membrane decreased by 15 % (from 5.6 ± 0.2 mS cm^{-1} to 4.7 ± 0.6 mS cm^{-1}) after cycling. The membranes themselves were clear and had no evidence of reddish color, suggesting that this drop in conductivity was not due to ingress of VO$_2^+$ ion (unlike the case of the ex-situ test). The ultimate tensile strength and the elongation at break were significantly reduced to 8.7 ± 2.2 MPa and 3.5 ± 0.6 %, respectively (from 19 ± 2 MPa and 18 ± 1.4 % initially). Identical peaks were seen in the 2-D HMQC NMR spectra before and after 100 hours of 20 charge/discharge cycles (Figure S8), however, from the ^{1}H NMR spectra (Figure S9), a 20% reduction in the number of cationic groups was deduced. From the post-test ^{1}H NMR spectrum, the IEC after was estimated to be 1.2 mmol g^{-1} (recall that the initial IEC was 1.5 mmol g^{-1}). Hence, there was significant degradation of cationic sites during in-situ VRFB operation, resulting in a decrease in ionic conductivity after 100 hours of testing.

We also observed a new peak at approximately 2.1 ppm that most probably corresponds to protons in the methyl groups attached to a tertiary amine.[74] The reduction of the peak at 3.1 ppm and the appearance of a new peak at 2.1 ppm confirm the demethylation of the quaternary ammonium groups (20% of initial groups) in the conditions encountered during the redox flow battery operation (presence of oxidizing VO_2^+ species and large cell voltages). Therefore, in addition to backbone degradation and concomitant loss in mechanical properties, some cation group degradation was also observed during flow-battery testing. At this stage, we can confirm that VRFB cycling presents a much more aggressive environment to the AEM than mere exposure to an oxidizing VO_2^+ solution. This has also been previously reported in the literature.[40] We suggest that researchers should not rely exclusively on the latter test to claim AEM stability.

Conclusions

Cardo-polyetherketone (PEK-C) based anion exchange membranes were prepared by chloromethylation of PEK-C followed by reaction with trimethylamine. The existence of quaternary ammonium groups in the membrane was confirmed by ^1H NMR and FTIR spectroscopy. The ion exchange capacity (in sulfate counter-ion form) was determined by titration to be 1.4 ± 0.2 mmol g^{-1}. The liquid–phase water uptake of this AEM was 36 ± 2 wt%. The sulfate ion conductivity and the vanadium (IV) permeability at 30°C were 5.6 ± 0.5 mS cm^{-1} and $8.2\pm0.2 \times10^{-9}$ cm^2 s^{-1}. Themogravimetric analysis confirmed the stability of the anion exchange membrane up to 260°C. The glass transition temperature determined by differential scanning calorimetry and dynamic mechanical analysis was between 221°C and 229°C. The ultimate tensile strength, elongation at break and Young's modulus were 19 ± 2 MPa, $18.1\pm1.4\%$ and 0.54 ± 0.03 GPa.

^1H NMR and ^1H-^{13}C heteronuclear multiple-quantum correlation spectroscopy were used to probe any changes in chemical structure of the anion exchange membrane upon exposure to highly oxidizing VO_2^+ solution. After immersion in VO_2^+ solution for 1500 hours, the sulfate conductivity, ultimate tensile strength, elongation at break and Young's modulus of QPEK-C-TMA$^+$ SO$_4^{2-}$ decreased to 4.3 ± 0.7 mS cm^{-1}, 12 ± 1 MPa, 8.3 ± 1.4 % and 0.49 ± 0.04 GPa, respectively. The loss in conductivity was attributed to vanadium ion ingress into the membrane, and was reversible upon rinsing the membrane in acidic solutions. No change in IEC was observed.

GPC was used to measure the molecular weights (Mn and Mw) of QPEK-C-TMA$^+$ before and after the stability test. The initial molecular weights were 38,500 and 90,700, respectively, whereas the molecular weights subsequent to the stability test were 31,100 and 73,700. The observed loss in the mechanical properties was attributed to the reduction in molecular weight due to backbone degradation.

This AEM was used to prepare a single-cell vanadium redox flow battery, which was tested for 100 hours using a charge-discharge protocol. The current and energy efficiencies (at 30 mA cm^{-2}) were in the range 97-99% and 80-82 %, respectively. Postmortem analysis of the membrane after testing in a vanadium redox flow battery for 100 h also indicated a decrease in membrane ionic conductivity and ultimate tensile strength (to 4.7 ± 0.6 mS cm^{-1}, and 9 ± 2 MPa). However, in this case, the loss in conductivity was not reversible. NMR analysis confirmed that 20% of the cation sites in the AEM were degraded. These results suggested that while ex-situ tests may well indicate high chemical stability, they may not adequately capture the degradation modes prevalent in an operating VRFB during charge-discharge cycling, especially on the chemical stability front. In general, the properties shown by the PEK-C based AEM were promising and this material is presented as a viable separator membrane for VRFBs, albeit needing more attention devoted to enhancing chemical stability.

Note

Center for Electrochemical Science and Engineering, Department of Chemical and Biological Engineering, Illinois Institute of Technology, Chicago, IL 60616 (USA)

*Corresponding author's e-mail: ramani@iit.edu

Acknowledgements

References

1. M. Schreiber, M. Harrer, A. Whitehead, H. Bucsich, M. Dragschitz, E. Seifert and P. Tymciw, *J. Power Sources*, 2012, 206, 483-489.
2. K. J. J. Ming, N. Yu, I. A. Karimi and D.-Y. Lee, *Ind. Eng. Chem. Res.*, 2013, 52, 142-151.
3. M. Skyllas-Kazacos, M. H. Chakrabarti, S. A. Hajimolana, F. S. Mjalli and M. Saleem, *J. Electrochem. Soc.*, 2011, 158, R55-R79.
4. B. Dunn, H. Kamath and J.-M. Tarascon, *Science (Washington, DC, U. S.)*, 2011, 334, 928-935.
5. G. Kear, A. A. Shah and F. C. Walsh, *Int. J. Energy Res.*, 2012, 36, 1105-1120.
6. d. L. C. Ponce, A. Frias-Ferrer, J. Gonzalez-Garcia, D. A. Szanto and F. C. Walsh, *J. Power Sources*, 2006, 160, 716-732.
7. B. Schwenzer, J. Zhang, S. Kim, L. Li, J. Liu and Z. Yang, *ChemSusChem*, 2011, 4, 1388-1406.
8. E. Sum and M. Skyllas-Kazacos, *J. Power Sources*, 1985, 15, 179-190.
9. D. Chen, M. A. Hickner, E. Agar and E. C. Kumbur, *Electrochem. Commun.*, 2013, 26, 37-40.
10. X. Lin, M. Gong, Y. Liu, L. Wu, Y. Li, X. Liang, Q. Li and T. Xu, *J. Membr. Sci.*, 2013, 425-426, 190-199.

11. M. Skyllas-Kazacos, D. Kasherman, D. R. Hong and M. Kazacos, *J. Power Sources*, 1991, 35, 399-404.

12. W. Wang, S. Kim, B. Chen, Z. Nie, J. Zhang, G.-G. Xia, L. Li and Z. Yang, *Energy Environ. Sci.*, 2011, 4, 4068-4073.

13. US20120077067A1, 2012.

14. X. Wei, L. Li, Q. Luo, Z. Nie, W. Wang, B. Li, G.-G. Xia, E. Miller, J. Chambers and Z. Yang, *J. Power Sources*, 2012, 218, 39-45.

15. US20100261070A1, 2010.

16. EP312875A1, 1989.

17. H. Izawa, T. Hiramatsu and S. Kondo, *Proc. Intersoc. Energy Convers. Eng. Conf.*, 1986, 21st, 1018-1021.

18. D. A. Johnson and M. A. Reid, *J. Electrochem. Soc.*, 1985, 132, 1058-1062.

19. D. P. Scamman, G. W. Reade and E. P. L. Roberts, *J. Power Sources*, 2009, 189, 1220-1230.

20. H. Zhou, H. Zhang, P. Zhao and B. Yi, *Electrochim. Acta*, 2006, 51, 6304-6312.

21. J. Cheng, L. Zhang, Y.-S. Yang, Y.-H. Wen, G.-P. Cao and X.-D. Wang, *Electrochem. Commun.*, 2007, 9, 2639-2642.

22. P. K. Leung, d. L. C. Ponce and F. C. Walsh, *Electrochem. Commun.*, 2011, 13, 770-773.

23. Z. Xie, D. Zhou, F. Xiong, S. Zhang and K. Huang, *J. Rare Earths*, 2011, 29, 567-573.

24. P. K. Leung, C. Ponce-de-Leon, C. T. J. Low, A. A. Shah and F. C. Walsh, *J. Power Sources*, 2011, 196, 5174-5185.

25. S. Kim, J. Yan, B. Schwenzer, J. Zhang, L. Li, J. Liu, Z. Yang and M. A. Hickner, *Electrochem. Commun.*, 2010, 12, 1650-1653.

26. X. Li, H. Zhang, Z. Mai, H. Zhang and I. Vankelecom, *Energy Environ. Sci.*, 2011, 4, 1147-1160.

27. H. Zarrin, J. Wu, M. Fowler and Z. Chen, *J. Membr. Sci.*, 2012, 394-395, 193-201.

28. Q. Luo, H. Zhang, J. Chen, P. Qian and Y. Zhai, *J. Membr. Sci.*, 2008, 311, 98-103.

29. T. Mohammadi and M. Skyllas-Kazacos, *J. Membr. Sci.*, 1995, 98, 77-87.

30. G.-J. Hwang and H. Ohya, *J. Membr. Sci.*, 1997, 132, 55-61.

31. F. Zhang, H. Zhang and C. Qu, *J. Phys. Chem. B*, 2012, 116, 9016-9022.

32. H. Prifti, A. Parasuraman, S. Winardi, T. M. Lim and M. Skyllas-Kazacos, *Membranes (Basel, Switz.)*, 2012, 2, 275-306.

33. D. Xing, S. Zhang, C. Yin, C. Yan and X. Jian, *Mater. Sci. Eng., B*, 2009, 157, 1-5.

34. B. Zhang, S. Zhang, D. Xing, R. Han, C. Yin and X. Jian, *J. Power Sources*, 2012, 217, 296-302.

35. M.-s. J. Jung, J. Parrondo, C. G. Arges and V. Ramani, *J. Mater. Chem. A*, 2013, 1, 10458-10464.

36. F. Zhang, H. Zhang and C. Qu, *J. Phys. Chem. B*, 2012, 116, 9016-9022.

37. J. Pan, S. Lu, Y. Li, A. Huang, L. Zhuang and J. Lu, *Adv. Funct. Mater.*, 2010, 20, 312-319.

38. C. G. Arges and V. Ramani, *Proceedings of the National Academy of Sciences of the United States of America*, 2013, 110, 2490-2495.

39. M. Tanaka, K. Fukasawa, E. Nishino, S. Yamaguchi, K. Yamada, H. Tanaka, B. Bae, K. Miyatake and M. Watanabe, *J. Am. Chem. Soc.*, 2011, 133, 10646-10654.

40. D. Chen, S. Kim, L. Li, G. Yang and M. A. Hickner, *RSC Adv.*, 2012, 2, 8087-8094.

41. J. Fang and P. K. Shen, *J. Membr. Sci.*, 2006, 285, 317-322.

42. L. Li and Y. Wang, *J. Membr. Sci.*, 2005, 262, 1-4.

43. X. Yan, G. He, S. Gu, X. Wu, L. Du and H. Zhang, *J. Membr. Sci.*, 2011, 375, 204-211.

44. S. Xu, G. Zhang, Y. Zhang, C. Zhao, W. Ma, H. Sun, N. Zhang, L. Zhang, H. Jiang and H. Na, *J. Power Sources*, 2012, 209, 228-235.

45. S. Xu, G. Zhang, Y. Zhang, C. Zhao, W. Ma, H. Sun, N. Zhang, L. Zhang, H. Jiang and H. Na, *J. Power Sources*, 2012, 209, 228-235.

46. E. H. Yu, X. Wang, U. Krewer, L. Li and K. Scott, *Energy Environ. Sci.*, 2012, 5, 5668-5680.

47. T. Mohammadi and M. S. Kazacos, *J. Appl. Electrochem.*, 1997, 27, 153-160.

48. S. Zhang, C. Yin, D. Xing, D. Yang and X. Jian, *J. Membr. Sci.*, 2010, 363, 243-249.

49. P. K. Leung, Q. Xu, T. S. Zhao, L. Zeng and C. Zhang, *Electrochim. Acta*, 2013, 105, 584-592.

50. J. C. Jansen and E. Drioli, *Vysokomol. Soedin., Ser. A Ser. B*, 2009, 51, 2101-2112.

51. L. Jia, X. Xu, H. Zhang and J. Xu, *J. Appl. Polym. Sci.*, 1996, 60, 1231-1237.

52. J. H. Chen, Q. L. Liu, A. M. Zhu, J. Fang and Q. G. Zhang, *J. Membr. Sci.*, 2008, 308, 171-179.

53. J. H. Chen, Q. L. Liu, Y. Xiong, Q. G. Zhang and A. M. Zhu, *J. Membr. Sci.*, 2008, 325, 184-191.

54. C. Akiba, K. Watanabe, K. Nagai, Y. Hirata and Q. T. Nguyen, *Journal of Applied Polymer Science*, 2006, 100, 1113-1123.

55. A. Basile, L. Paturzo, A. Iulianelli, I. Gatto and E. Passalacqua, *J. Membr. Sci.*, 2006, 281, 377-385.

56. Y. Xiong, Q. L. Liu and Q. H. Zeng, *J. Power Sources*, 2009, 193, 541-546.

57. S. Gu, R. Cai, T. Luo, K. Jensen, C. Contreras and Y. Yan, *ChemSusChem*, 2010, 3, 555-558.

58. J. Fang and P. K. Shen, *J. Membr. Sci.*, 2006, 285, 317-322.

59. W. Ma, C. Zhao, H. Lin, G. Zhang and H. Na, *J. Appl. Polym. Sci.*, 2011, 120, 3477-3483.

60. E. Avram, E. Butuc, C. Luca and I. Druta, *J. Macromol. Sci., Pure Appl. Chem.*, 1997, A34, 1701-1714.

61. C. G. Arges and V. Ramani, *J. Electrochem. Soc.*, 2013, 160, F1006-F1021.

62. Q. Zhang, Q. Zhang, J. Wang, S. Zhang and S. Li, *Polymer*, 2010, 51, 5407-5416.

63. B. Sun and M. Skyllas-Kazacos, *Electrochim. Acta*, 1992, 37, 1253-1260.

64. Z. Liu, X. Li, K. Shen, P. Feng, Y. Zhang, X. Xu, W. Hu, Z. Jiang, B. Liu and M. D. Guiver, *J. Mater. Chem. A*, 2013, 1, 6481-6488.

65. T. D. W. Claridge, *Elsevier Science*, 2008, 27.

66. X. Lin, Y. Liu, S. D. Poynton, A. L. Ong, J. R. Varcoe, L. Wu, Y. Li, X. Liang, Q. Li and T. Xu, *J. Power Sources*, 2013, 233, 259-268.

67. E. Mahendiravarman and D. Sangeetha, *Int. J. Hydrogen Energy*, 2013, 38, 2471-2479.

68. J. S. Lawton, A. Jones and T. Zawodzinski, *J. Electrochem. Soc.*, 2013, 160, A697-A702.
69. Y. Shiokawa, H. Yamana and H. Moriyama, *J. Nucl. Sci. Technol.*, 2000, 37, 253-256.
70. K. D. Kreuer, *J. Membr. Sci.*, 2001, 185, 29-39.
71. W. Liu, T. Chen and J. Xu, *J. Membr. Sci.*, 1990, 53, 203-213.
72. D. Chen, M. A. Hickner, E. Agar and E. C. Kumbur, *ACS Appl Mater Interfaces*, 2013.
73. D. Chen and M. A. Hickner, *Phys. Chem. Chem. Phys.*, 2013, 15, 11299-11305.

The stability of cardo-poly(etherketone) based anion exchange membranes was investigated by performing 1-D and 2-D HMQC NMR spectroscopy.